Chapter 6

Investigation of Synergistic effect in PBTTT/DPPCN hybrid material towards enhancing the field effect mobility and Photosensitivity

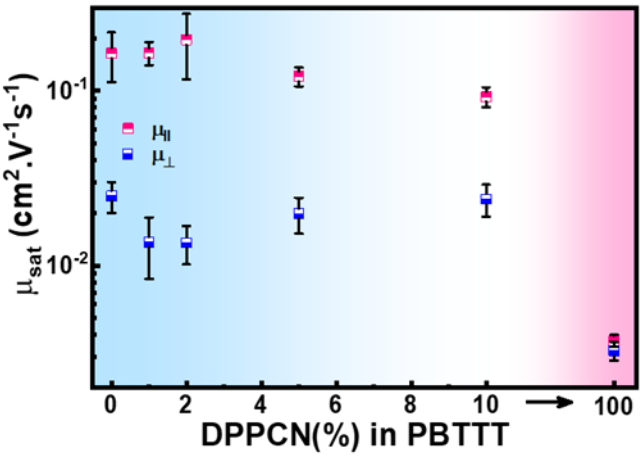

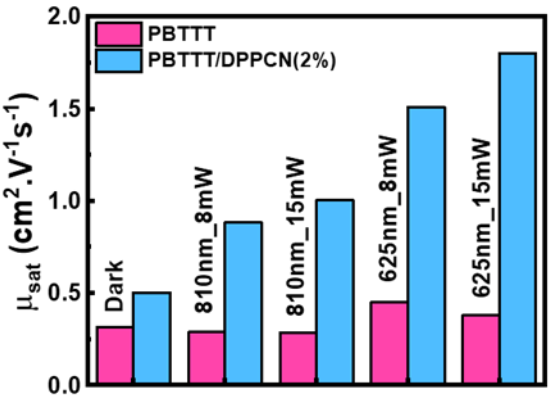

6.1.Introduction

Near-infrared (NIR) photodetectors have received huge scientific curiosity in several fields, such as bioimaging, low radiation detection, and other medical applications, including critical health monitoring [179–181]. For this purpose, organic-based photodetectors, especially organic phototransistors (OPTs), are being extensively explored owing to their striking features of low-cost solution-processing compatibility, easy functionalization, and mechanical flexibility [42]. Organic phototransistors (OPTs) are organic field effect transistors (OFETs) that combine the effect of photovoltaic and photoconduction. When the photogenerated excitons tend to diffuse through the semiconductor bulk, they often dissociate into free charge carriers at the donor/acceptor interface (for donor/acceptor composite material) or near the built-in field of the depletion regime [42,182,183] or under the effect of an external applied electric field. Thus, the additional photogenerated charge carriers will drift along with the gate bias-induced accumulated charges at the semiconductor/insulator interface under the effect of the lateral applied electric field in the channel, and thus, eventually alters/increases the effective carrier mobility [184].

Now, effective absorption of NIR photons, high photoconversion efficiency, and carrier mobility are the key features a material should have to be used as an active material [41]. Thus, narrow band-gap organic molecules with easy solution processability could be good candidates for this application. Organic molecules having band-gap in the NIR range are prone to lattice distortions, which may lead to a smaller exciton diffusion length and poor device performance.

One of the solutions to the challenges, as mentioned earlier, is to use a blend of two or more organic semiconducting materials [40,183]. Harnessing the key advantages of individual materials, significant improvement in electronic and optoelectronic functionality can be

achieved. This synergistic approach has been utilized in several fields, like bulk heterojunction solar cells, OFETs, organic light-emitting diodes, and even organic photodetectors [185–192]. It has been proved that a larger local free volume facilitates the self-organization and crystallization process [48]. For this reason, we have adopted PBTTT having rotational invariance in its backbone that helps to adopt a low-energy planar backbone conformation and promotes the self-assembly process, minimizes steric hindrance from adjacent side chains, and enhances the crystalline order. Furthermore, for photo absorption in the NIR range, we have utilized a novel diketopyrrolopyrrole (DPP) based NIR dye molecule DPPCN [193].

Nevertheless, organic-based electronic devices lack stability, reproducibility, and an operational lifetime to compete with commercially available inorganic devices. Thus, to make organic-based devices commercially viable, there are two most suitable approaches: one is to reduce the manufacturing cost, and second, to improve device performance.

One of the major costs in manufacturing organic electronic devices originated from film fabrication. Although complex and multistep synthesis and refinement make the active material costly, wastage of these materials while fabricating pin-hole-free, homogeneous, and large-area films increases the fabrication cost significantly. Thus, pronouncing low-cost production of organic electronics suggests that thin-film processing techniques are cheaper than inorganic counterparts [8]. To address this issue, we have adopted a low-cost and facile thin-film fabrication method named “Floating-film transfer method (FTM)” that minimizes the material wastage by up to ~95% and provides a high-quality active layer suitable for OPT application [56,57,67,160]. The following and equally important criterion for the realization of this technology is the performance of these devices. Since the inherent chemical structure and intra-molecular interaction is difficult to alter in organic

semiconducting polymers (OSPs), we can tune the inter-molecular interactions by modifying their crystal packing and orientation. The degree of crystallinity may increase by incorporating filler templates or directed self-assembly, which may lead to better device performance by altering their electronic properties [194,195]. In our study, an optimum amount of DPPCN in the PBTTT matrix has been shown to improve both the crystallinity and unidirectional molecular orientation, which momentarily enhanced the average field effect mobility up to 0.2 cm^2/Vs. Moreover, due to charge transfer interaction, the blended system was found to show improved photosensitivity around 2.8×10^3 in the NIR region (810 nm_LASER) and 2.2×10^4 in red light (625 nm_LASER). Thus, controlled improvement in materials stability, crystallinity, carrier mobility, and photo response through a synergistic effect between a rigid conjugated polymer backbone (PBTTT) and a NIR dye molecule (DPPCN) may open up new possibilities in the field of organic electronics.

6.2.Results and Discussion

6.2.1. Characterizations of hybrid polymer ink

At first, the synthesis of the hybrid polymer ink was monitored through UV-vis and FT-IR spectroscopy. The color of the pinkish PBTTT solution turns into a light bluish-pink solution (PBTTT/DPPCN solution) after 24 hours of constant stirring, slow drying, and redissolution process. While characterized through the UV-vis spectroscopy (shown in Figure 6.1 (a)), almost featureless PBTTT spectra ($\lambda_{max} = 482$ nm) start showing a vibration shoulder peak located at 584 nm, which can be originated due to slight aggregation, i.e., improvement in interchain π-π stacking in the PBTTT solution [194,196–198]. With increasing the DPPCN concentration, a small hump starts appearing at 715 nm, but the absorption maxima, λ_{max} for DPPCN, lies at 690 nm. It signifies that the small

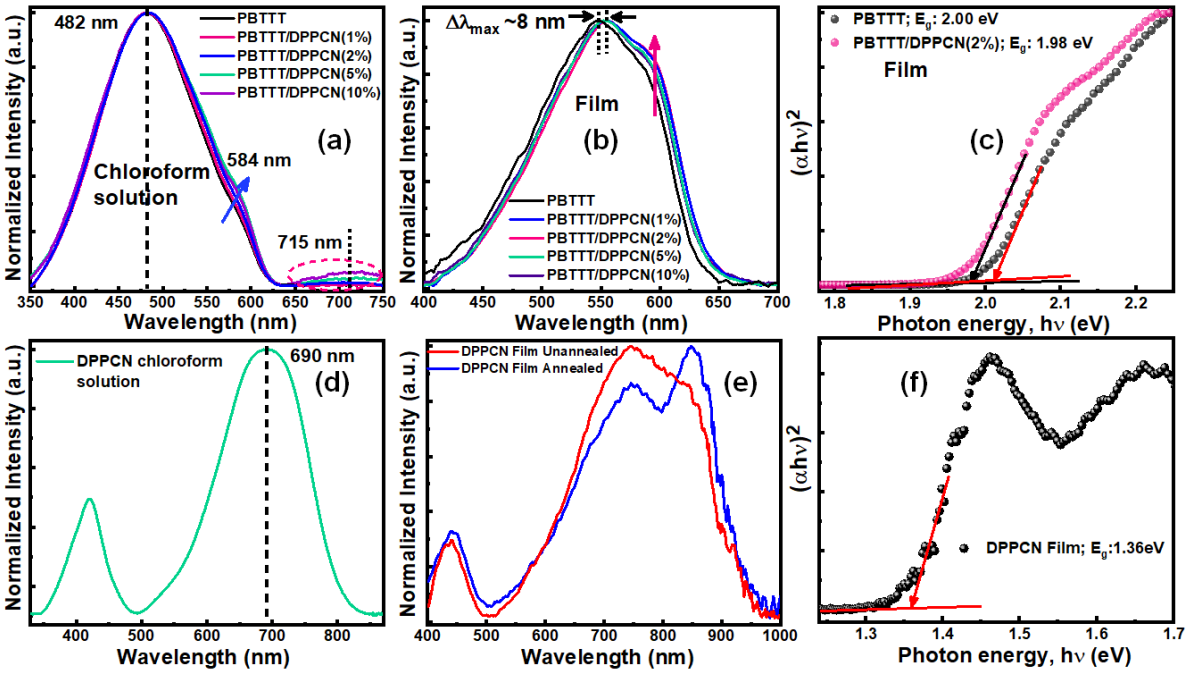

Figure 6.1 (a) Non-polarized UV-vis spectra of pristine PBTTT, pristine DPPCN, and hybrid materials in solution (a), & (d), and in film (b) and (e), and the band-gap estimation in annealed thin films of (C) pristine PBTTT and PBTTT/DPPCN(2%) and in pristine DPPCN (f).

hump, shown by a red circle in the absorption spectra, corresponds to DPPCN, and a spectral shift of ~25 nm suggests the interaction between PBTTT and DPPCN in the solution phase.

In order to confirm the synthesis of PBTTT/DPPCN polymer hybrid ink and the interaction between them, the molecular structure and functionality of pristine PBTTT, DPPCN, and PBTTT/DPPCN(2%) ink was investigated through FT-IR in ATR mode, as shown in Figure 6.2 (d). All the bands characteristic of the PBTTT and DPPCN with different functional groups and moieties have been tabulated in TABLE 6.1. The FT-IR spectrum of the hybrid polymer ink displayed the appearance of -C≡N nitrile-stretch [199] at 2216 cm^{-1} with a low-frequency shift of ~7 cm^{-1} as compared to the parent DPPCN molecule (2223 cm^{-1}). This shift suggests the electron density change in DPPCN molecule, which can be used as a signature of the interaction between PBTTT and DPPCN through some non-

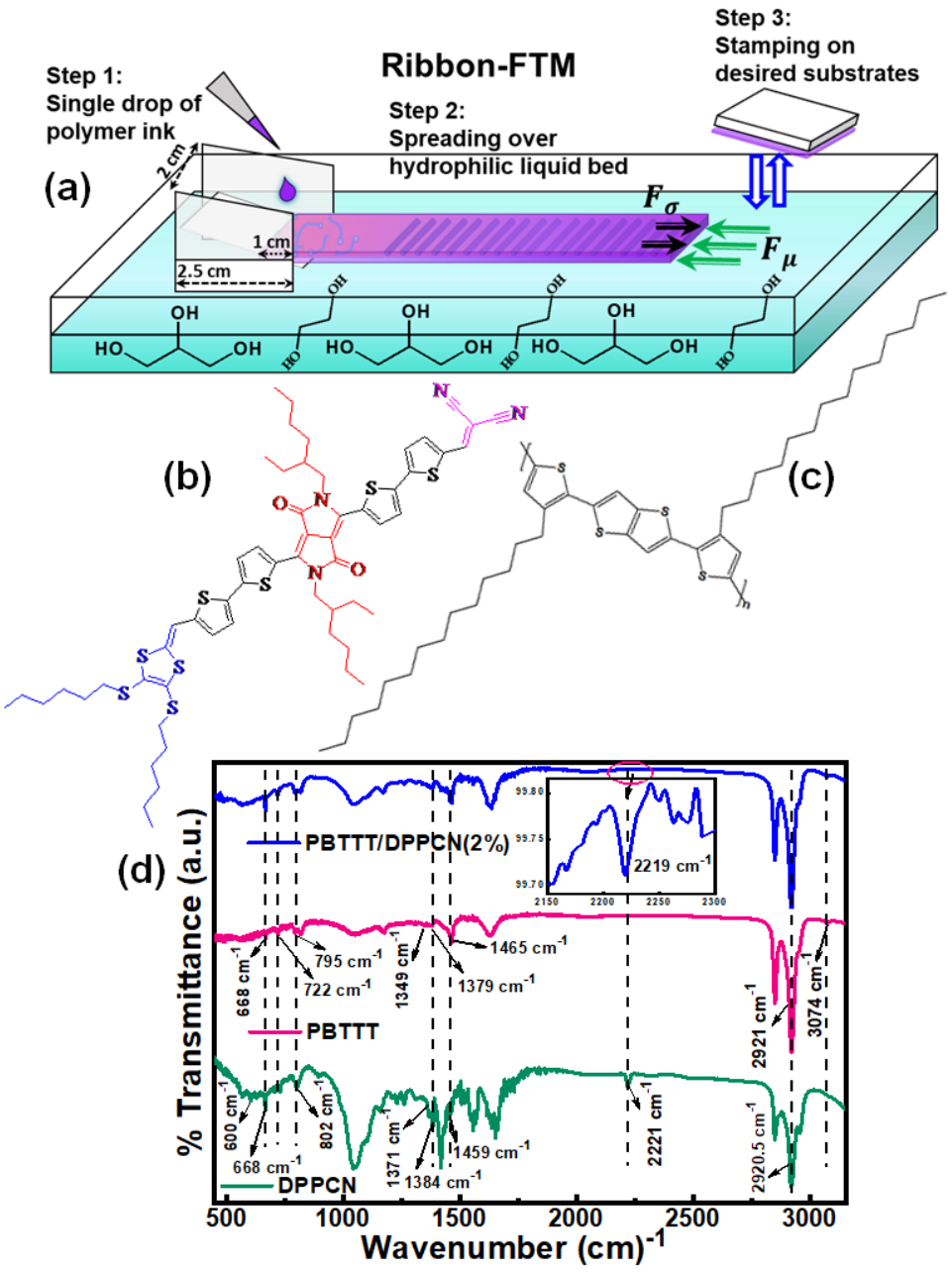

Figure 6.2 Schematic representation of the film formation process through ribbon-FTM (a) and the utilized organic molecules DPPCN(b) and PBTTT(c), and (d) represents FTIR spectra of pristine PBTTT, DPPCN and PBTTT/DPPCN(2%).

covalent secondary interactions [195]. All other characteristic peaks of PBTTT are present in the hybrid ink with some little positional shift, which may be the effect of chemical environment change of the functional moieties [199–203].

6.2.2. Characterizations of FTM films

After optimizing all the dominating film fabrication factors, as described in the experimental part, large-area (~40 cm^2, Figure 2.1 (b)) FTM films were fabricated utilizing the as- prepared polymer inks through a methodology schematically illustrated in Figure 6.2 (a). The as-prepared films deposited over quartz glass substrate were first characterized through a non-polarized UV-vis spectroscopy at RT (300 K), shown in Figure 6.1 (b). The absorption maxima for PBTTT film were found to be highly red-shifted ($\Delta\lambda_{max} = 65$ nm) as compared to its solution phase, as planar PBTTT backbones go for highly ordered self-assembled structures in the solid phase [48,56]. Now, after doping with DPPCN molecules, again a bathochromic spectral shift was found in the absorption maxima, $\Delta\lambda_{max} = 8$ nm

TABLE 6.1 List of different functional groups found in pristine PBTTT, DPPCN and PBTTT/DPPCN(2%).

Band assignment	**Vibration frequency in cm^{-1}**		
	DPPCN	**PBTTT**	**PBTTT/DPPCN(2%)**
-C-H stretch of aromatic proton within thiophene ring [203]		3074	3073
-C-H stretch in main chain [203]	2920.5	2921	2920.8
-C≡N nitrile-stretch [199]	2223		2216
Stretching modes of C=C and C-C within thiophene ring [202,203]	1459, 1384, 1371	1465, 1379, 1349	1465, 1384,1341
-C-H out-of-plane vibration within thiophene ring [201]	802	795	797
C-H bending within thiophene ring [203]		722	719
Characteristic of thiophene moiety [203]		668	668
C-S-C stretching [200,203]	605		590

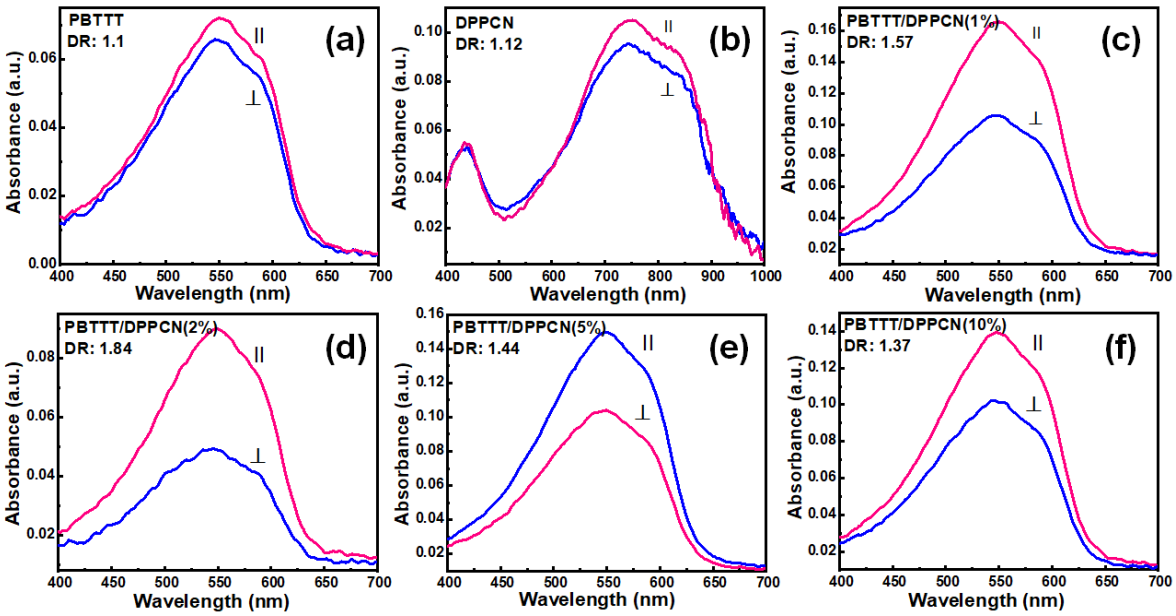

Figure 6.3 Polarized optical absorption spectra of the as-prepared thin films of PBTTT (a), DPPCN (b), and PBTTT/DPPCN hybrids (c, d, e, & f).

because of the increase in effective π-conjugation length. Moreover, gradual growth in the vibronic shoulder peak located at λ = 590 nm could be noticeable, with the highest growth in PBTTT/DPPCN(2%) case. As highly crystalline-oriented PBTTT domains cause the growth in the vibronic shoulder [194,204], this finding suggests that the degree of π-orbital overlap among the proximate PBTTT molecules is highest in 2% doping case. Next, for a qualitative study of the aggregation type in the hybrid polymer matrix, we have adopted the Spano's weakly interacting H-aggregate model [136], that vastly utilized for P3HT and sometimes used in PBTTT [204,205]. Thus, applying Spano's model, we found that all the PBTTT films show H-type inter-chain interaction, as absorption intensity ratio, $R_{abs}(= A_{0-0}/A_{0-1})$ <1 for both pristine and doped films, as shown in Figure 6.9 (d). Further, due to inter-band mixing in these oriented domains, R_{abs} is interrelated to the intramolecular vibration energy (taking the same as P3HT, $\hbar\omega_0 \sim 0.18\ eV$ [205]), and free exciton bandwidth (W) (taking Huang–Rhys factor, $HR = 1$) as per equation 4.5. W is

directly related to the degree of crystallinity as well as electronic property of materials. The value of *W* estimated to be 53.9 meV for PBTTT film and it starts decreasing with

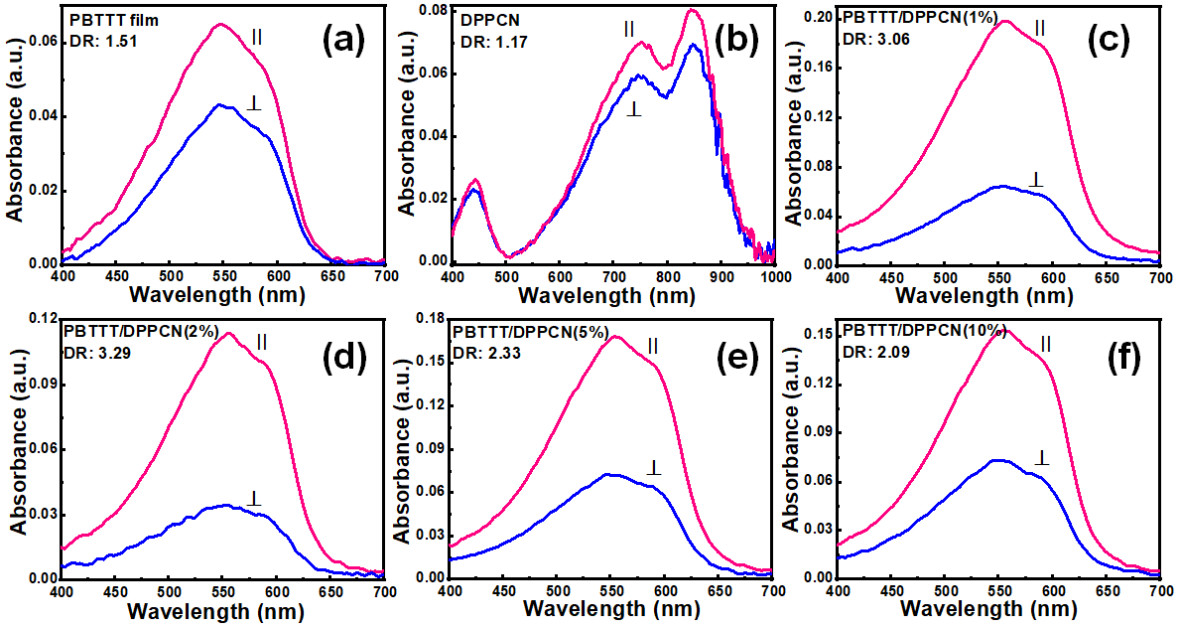

Figure 6.4 Polarized optical absorption spectra of the annealed thin films of PBTTT (a), DPPCN (b), and PBTTT/DPPCN hybrids (c, d, e, & f).

increasing the doping concentration of DPPCN and reaches to the lowest at 29.4 meV with 2% DPPCN and then again it starts increasing with further doping. As, lower the value of *W*, lower will be the interchain excitonic coupling, thus with the lowest *W* value, an improved electronic as well as photovoltaic response is expected for the PBTTT/DPPCN(2%) case. The optical band gap (E_g), i.e., energy required for the photoexcited lowest electronic transition (Figure 6.1 (c)) is found to be decreased in PBTTT/DPPCN(2%) case (1.98 eV) compared to the pristine PBTTT film (2.00 eV).

Now, for the realization of high-performing planar electronic devices, apart from increasing the effective carrier concentration through hole dopant, we have focused on extending the uniaxially oriented domain size in PBTTT semicrystals through FTM. Thus, to quantify the degree of molecular orientation in as-prepared films, we have characterized them through

polarized electronic absorption spectroscopy and estimated the value of dichroic ratio, DR. As, transition dipole moment for photoinduced electronic transition (0-1) aligned along the electron-rich conjugated PBTTT backbone, incident light polarized parallel to the polymer backbone direction will give rise to the highest optical absorption and reaches a minimum at the orthogonal position. Now, average DR of as-prepared films was estimated around 1.1 (lowest) in pristine PBTTT film, 1.12 in DPPCN film, and 1.84 (highest) in PBTTT/DPPCN(2%) case, as shown in Figure 6.3. Interestingly, after annealing at 100 °C for 1 hour, DR found to further increased up to 1.51 in pristine film and 3.29 in the 2% doping case. This enhancement in molecular orientation can be explained through the absorbance spectra of annealed DPPCN film, as shown in Figure 6.4. After annealing, almost featureless DPPCN absorption spectra exhibit a bathochromic spectral shift along with a well-structured absorption profile (Figure 6.1 (e)). This result indicates that, after the controlled heat treatment, recrystallization of DPPCN molecules helps enlarge the oriented domain size of PBTTT lamellar stacking as well. The DR of PBTTT film may also increase further if we anneal the films above the liquid crystalline temperature (~180 °C) as reported by Nikita et al. [75]. However, due to the limitation of DPPCN degradation and our particular device structure (CYTOP glass transition temperature ~108 °C), we stopped at 100 °C.

6.2.3. Anisotropic charge transport

Next, to examine how DPPCN doping impacted the overall device performance and the planar anisotropic charge transport, multiple parallel and perpendicular OFETs were fabricated on Si/SiO_2 substrates coated with FTM films. All the OFETs were designed in a bottom gate top contact (BGTC) architecture because they offer comparatively lower contact resistance compared to the bottom gate bottom contact (BGBC) mode, as per the

reports by Bhargava et al. [32], where they simulated both the device architectures through the Poole-Frenkel mobility model considering hopping-based charge transport in organic disordered systems (rr-P3HT). The output characteristics ($I_{DS} - V_{DS}$) for parallel and

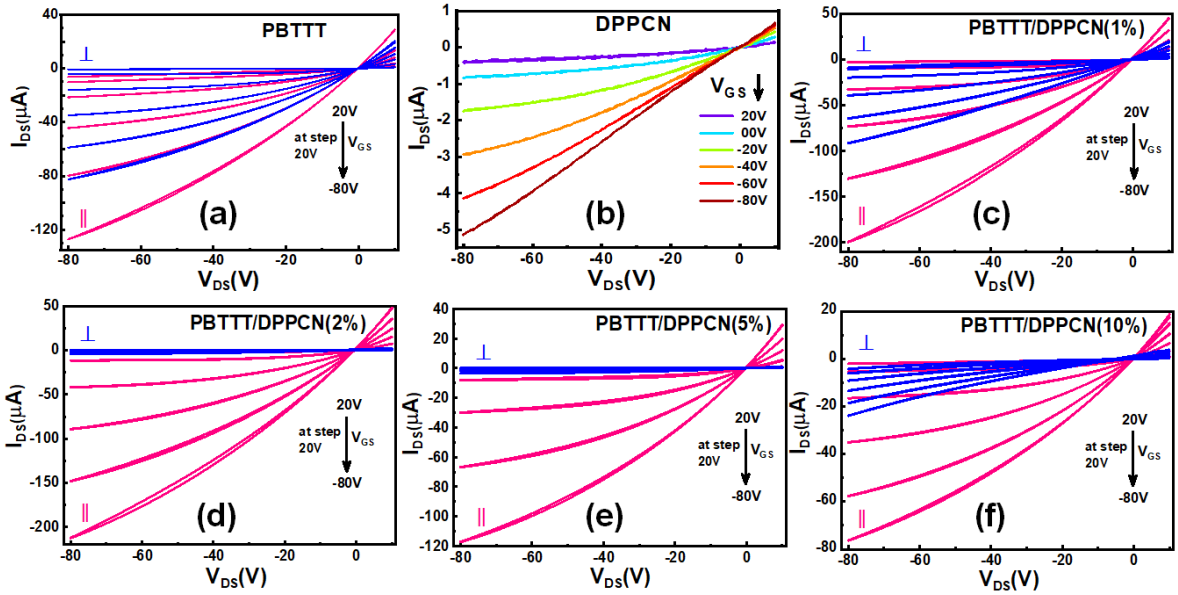

Figure 6.5 OFET output characteristics corresponding to pristine PBTTT (a), DPPCN (b), and PBTTT/DPPCN hybrids (c, d, e, & f).

perpendicular OFETs corresponding to both pristine and doped PBTTT have been shown in Figure 6.5, which clearly shows a unipolar p-type behavior. Moreover, a distinct change in $\|I_{DS}\ vs\ \perp I_{DS}$ is perceptible at each respective gate bias in all the OFETs except for DPPCN, which hardly suitable for OFET application in pristine form. The anisotropy in drain current follows the trend of optical DR. From 1.6 for pristine PBTTT, output drain current (at $V_{GS} = -80V$) starts increasing with increasing the doping percentage up to 51 in 2% DPPCN case, and then again decreases with further doping. The increase in drain current can be explained as the increase in hole concentration in PBTTT through charge transfer from PBTTT HOMO level to DPPCN HOMO. However, with a further increase in DPPCN concentration, the orientation, and overall film crystallinity decrease, as found in the optical results. Now, from the transfer characteristic curves shown in Figure 6.6,

saturation mobility (μ_{sat}) was estimated using a W/L ratio of 33.33 and basic transistor equations, as described earlier [56]. The maximum average saturation mobility is found to be 0.2 $cm^2V^{-1}s^{-1}$ at $V_{DS} = -80\ V$ for PBTTT/DPPCN(2%) case (with a highest mobility

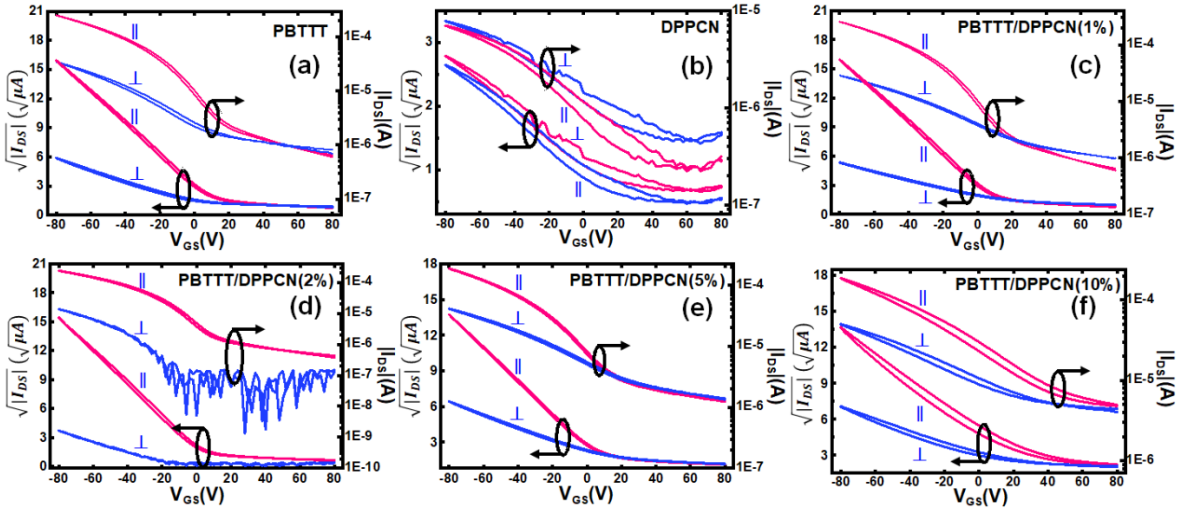

Figure 6.6 OFET transfer characteristics of pristine PBTTT (a), DPPCN (b), and PBTTT/DPPCN hybrids (c, d, e, & f).

value of 0.5 $cm^2V^{-1}s^{-1}$), which is almost 1.25 times the average saturation mobility for PBTTT, i.e., 0.16 $cm^2V^{-1}s^{-1}$. Moreover, with increasing the DPPCN concentration further, effective hole mobility decreases because of a higher degree of microstructural perturbations. The effect of structural disorder reflects in the hysteresis in transfer curves for 10% doping level. Similar to the output characteristics, the mobility anisotropy is found highest, ~25, in the 2% doping level, as evident from the perusal of Figure 6.9 (c). To standardize the OFET characteristics, multiple OFETs have been measured in similar conditions and the statistical distributions of field effect mobility in pristine PBTTT and PBTTT/DPPCN(2%), has been displayed in Figure 6.9 (b). Moreover, to investigate the device stability, three OFETs of each kind were kept under relative humidity level of 10-15% inside a glass desiccator in dark and were measured up to 150 days. The OFETs were found to retain almost 64%-67% of their initial field effect mobility even after 150 days, as shown in Figure 6.9 (a). As under biased condition, DPPCN is providing an energetically

favorable path for the charge carriers to percolate through channel as well as facilitates the carrier injection and collection through the electrode (Au), optimum percentage of DPPCN should enhance the optoelectrical functionality of OFETs without disturbing the uniaxial alignment of PBTTT backbone stacking.

6.2.4. Validation of electrical results

Thus, to validate the electrical performances, at first, the change in internal microstructural arrangement due to the introduction of optimum amount of DPPCN in pristine PBTTT has been investigated in terms of evolution in roughness topography. For this purpose, FTM films of PBTTT and PBTTT/DPPCN(2%) has been studied through AFM and Kelvin probe force microscopy (KPFM) in a 5×5 μm^2 scan area in non-contact tapping mode. From the surface roughness profile, as shown in Figure 6.7 (a) & (b), although aligned polymer chains are not clearly visible, but it shows polymer lamellar alignment at a macroscopic level. The 2D FFT (Fast Fourier transform) corresponding to the height profile (shown in the inset) shows a general isotropic nature of both films, however, there can be seen a shift from purely isotropic circular distribution to a elliptical one in the case of PBTTT/DPPCN(2%) film. This change in 2D FFT image suggests anisotropic surface features, i.e., more aligned domains found in the hybrid film. After analyzing the normalized probability density function of surface heights, we found that, the pristine polymer film is smoother (RMS roughness, $\boldsymbol{R_{rms}}$ ~1.99 nm) as compared to the hybrid film ($\boldsymbol{R_{rms}}$ ~2.27 nm), and they both follow a Gaussian distribution. This can be explained as the degree of aggregation and average coherence length is higher in case of PBTTT/DPPCN(2%) film.

As the objective of this study was to establish the correlation between film morphology and aligned crystalline domains with the device performance, further, the topographical

evolution in surface potential due to DPPCN doping has been examined through work function mapping. By applying a potential bias of 1V, KPFM mapped the surface potential distribution utilizing the electrostatic interaction between FTM film surface and conducting AFM tip in amplitude modulation mode. In Figure 6.7 (c) & (d), a clear variation in the

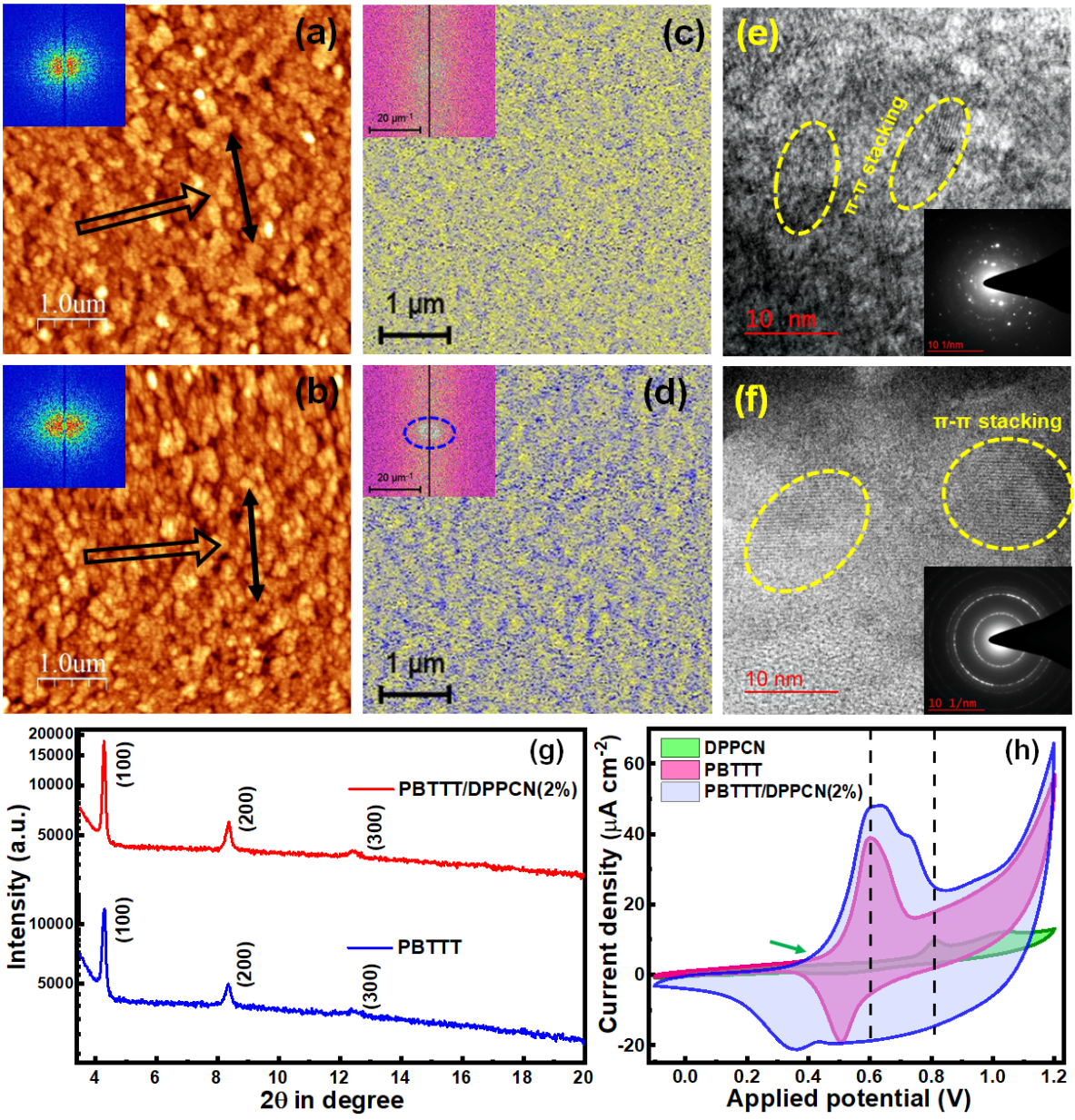

Figure 6.7 AFM height profile and KPFM scan along with corresponding 2D FFT in the inset for PBTTT (a & c) & PBTTT/DPPCN(2%) (b & d); Molecular orientation (double arrow) and film progression direction (single arrow) that has been estimated through the transparent polarizer sheet, is shown in the AFM images; Next, the HR-TEM images and corresponding SAED patterns has been shown for PBTTT (e) and PBTTT/DPPCN(2%) (f); Further, thin film XRD (g) and cyclic voltammetry (h) of the same systems has been shown.

distribution of contact potential difference (V_{CPD}) can be seen, which suggests a change in electronic property of the films after doping with DPPCN. To validate the anisotropic features, we have first decomposed the V_{CPD} signals into its harmonic components, and then the absolute values of the complex Fourier coefficients (modulus) mapped into a 2D FFT image (utilizing the Gwyddion software), as shown in the inset of Figure 6.7 (c) & (d). From these images, a clear anisotropic domain alignment is evident in PBTTT/DPPCN(2%) film (shown by blue circle at the center). Moreover, the average V_{CPD} found lower (~5.79 mV) in the hybrid film, as compared to the pristine one (~5.91 mV). This collective results suggest a easier charge migration is likely through the semiconductor-electrode interface for the PBTTT/DPPCN(2%) case.

Next, to study the effect of DPPCN doping in PBTTT, on the macromolecular arrangement and film crystallinity, out-of-plane meridional XRD scans were recorded at grazing incidence (GI) angle fixed at 0.15°. Figure 6.7 (g) shows the out-of-plane XRD pattern corresponding to PBTTT and PBTTT/DPPCN(2%) FTM films stamped over single oriented (001) Si substrates. As the scattering vector (χ) lies almost perpendicular to the substrate during the measurement, finding a set of (*h*00) diffraction peaks up to third order suggests the 'edge-on' type molecular packing in both the films. That means, the C-14 alkyl side-chains of PBTTT lies perpendicular to the substrate surface. The interplanar spacing, d_{h00} along the 'a-axis' i.e., alkyl stacking distance found to be similar in both films, 20.63Å and 20.59Å for PBTTT and PBTTT/DPPCN(2%) film, respectively. However, the average size of structurally coherent domains (L_c) was found to be extended up to 87.5 nm in PBTTT/DPPCN(2%) film as compared to the pristine polymer film (71.1 nm). The (100) diffraction peak intensity and corresponding FWHM in PBTTT/DPPCN(2%) film clearly signals the higher degree of structural coherence, which should facilitate the in-plane charge transport by delocalizing the π-electrons to a greater extent.

Further, at a sub-micrometer level, the local molecular arrangement in the pristine and hybrid polymer film was investigated through an HR-TEM at 200 kV energy after resolving the polymer burning issue by optimizing all the measuring conditions. The 2D projections of the molecular orientation in the as-prepared FTM films can be directly visualized in real space through HR-TEM. The bright-field HR-TEM images (Figure 6.7 (e) & (f)) of both films show lattice fringes (marked by yellow ring) consisting of alternating bright and dark lines with a period of 3.6±0.4Å and 3.7±0.1Å for PBTTT and PBTTT/DPPCN(2%) FTM films, respectively. This spacing is equivalent to the π-π stacking distance in PBTTT semicrystals [56,101], and thus the periodic contrast modulation originated from the successive stacking of electron-rich (due to sulfur atoms) conjugated PBTTT backbones in an 'edge-on' type molecular arrangement. M. Brinkmann et al. [87] also got similar features while studying directionally solidified P3HT semicrystals. Now, a closer look at the oriented domains reveals the presence of lattice bending at the domain boundaries, which restricts the growth of crystalline domains further. Moreover, this lattice bending also causes fluctuation in interplanar spacing (0.4Å and 0.1Å for PBTTT and PBTTT/DPPCN(2%) film) by introducing lattice strain, which momentarily disrupts the π-orbital overlap. Interestingly, this lattice disorder is prevalent in pristine PBTTT semicrystals, which is also reflected in the corresponding selected area electron diffraction (SAED) pattern, as shown in the inset. Usually, solution-processed flexible polymer films give concentric ring patterns in reciprocal space while diffracted through electron beam. However, the presence of multiple random dots, as well as more diffuse Scherrer rings, i.e., diffraction broadening in the SAED pattern, suggests lattice disorder dominates the local molecular arrangement in the pristine film. Nonetheless, a more precise ring pattern containing bright dots and a larger domain size (as shown in the bright field image)

evidenced a higher degree of π-electron delocalization in the PBTTT/DPPCN(2%) film, which justifies the charge transport results.

Now, to investigate the change in overall electronic band structure of PBTTT after doping with optimum percentage of DPPCN, cyclic voltammetry (CV) measurements have been

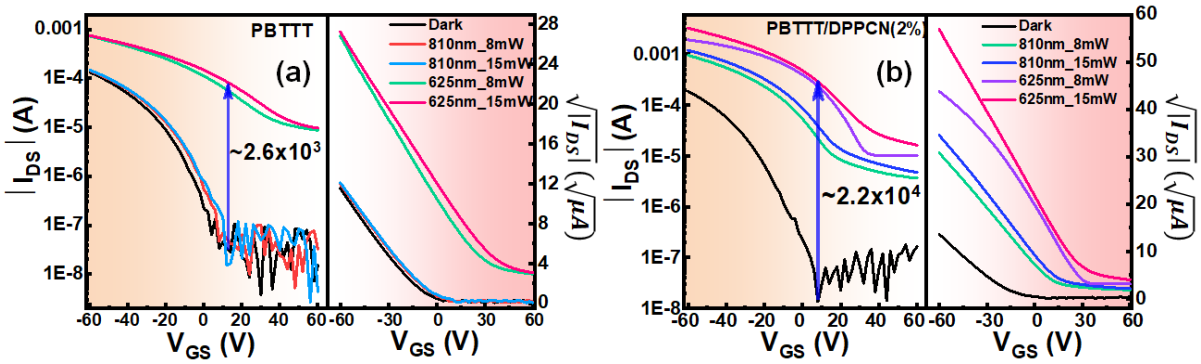

Figure 6.8 OFET photo-response for PBTTT (a) and PBTTT/DPPCN(2%) (b).

executed in a non-aqueous electrolyte (0.1 M Tetrabutyl ammonium perchlorate, TBAP in acetonitrile) utilizing a three-electrode system. For this measurement, working electrodes were prepared by three layers of FTM films lifted over masked conducting ITO substrates with a fixed geometrical active area of 0.5×0.5 cm^2, while a standard Ag/AgCl and coiled Platinum wire was used as reference and counter electrodes, respectively. Maintaining almost ideal measurement conditions, CV scans were recorded in the range of -0.1V to 1.2V in step of 2 mV @30 mV/s scan rate. Figure 6.7 (h) shows that the peak current has increased almost 1.25 times in doped film as compared to the pristine polymer film, that may have originated from the higher surface roughness [138]. Moreover, after doping with DPPCN, apart from the intrinsic first oxidation peak, another shoulder peak arises at a higher potential, suggesting the presence of some electronic levels at a lower energy than the PBTTT HOMO level. The oxidation onset also found in a lower potential side(~60 mV shift) than the pristine PBTTT film, signaling the reduction in ionization potential [196,206]. To evaluate the HOMO positions from the oxidation onsets (E_{ox}), we have used

the ferrocene reference ($E_{1/2(ferrocene)} = 0.405V$) and the standard equation [79], $E_{HOMO} = \left[\left(E_{ox} - E_{1/2(ferrocene)}\right) + 4.8\right] eV$. The estimated HOMO positions of PBTTT, DPPCN and PBTTT/DPPCN(2%) are -5.15 eV, -4.92 eV, and -4.86 eV, respectively. The DPPCN HOMO position properly matched with the theoretically calculated value [69]. So, doping with optimum percentage of DPPCN may have caused a structural rearrangement in PBTTT semicrystals, that delocalized the π-electron clouds to a greater extent, facilitating the electron removal process while interacting with electrolyte under biased condition [196,206]. Moreover, presence of new electronic levels nearer to the gold electrode work function (~5.0 eV) will provide an energetically easier step for the charge carriers to migrate. Thus, CV results reaffirms the findings from KPFM and XRD measurements and justifies the higher saturation mobility in PBTTT/DPPCN(2%) FTM films.

6.2.5. Photo-response study

Lastly, to investigate the photo response of the fabricated devices, LED lasers of wavelength 810 nm (NIR light) and 625 nm (red light) were used for illumination purposes. Transfer characteristics of the best-performing OFET were recorded in the dark and with two different laser power, 5 and 10 mW/cm^2. Figure 6.8, shows the transfer characteristics of parallel OFETs with PBTTT and PBTTT/DPPCN(2%) active layers in the dark and after illumination. From the perusal of Figure 6.8, it is evident that pristine PBTTT is non-responsive to NIR light because of a higher HOMO-LUMO gap, and the highest photosensitivity has been found around 2.6×10^3 under the red light of intensity 10 mW/cm^2. Interestingly, an optimum percentage doping of DPPCN in PBTTT results in 810 nm NIR detection with maximum photosensitivity of 2.8×10^3 at 10 mW/cm^2 intensity. Moreover, the photosensitivity of the system increased almost one order of magnitude towards the red

light of 10 mW/cm^2 intensity. This enhancement in device performance can be explained in terms of improved charge-transfer interaction. Under the illumination of light with proper energy, excitons are being formed in the semiconducting system, which further

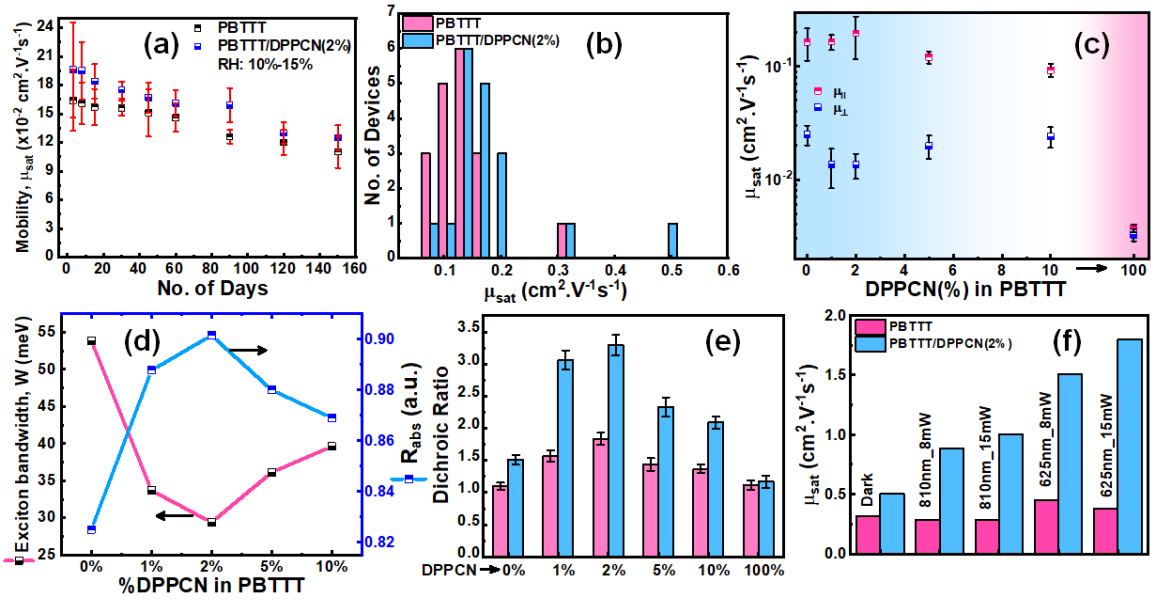

Figure 6.9 Represents OFET stability (a), statistical data of saturation mobility (b), mobility anisotropy (c), variation of exciton bandwidth along with R_{abs} value (d), optical anisotropy in terms of DR (e), and the photosensitivity with respect to the change in saturation mobility (f).

dissociates owing to the presence of built-in potential near the metal/semiconductor interface, which increases the carrier concentration (hole) in PBTTT and eventually enhances the effective field effect mobility of the system. Moreover, it has been proved that, due to the synergistic effect in PBTTT/DPPCN(2%) system, the structural order, as well as unidirectional molecular backbone arrangement, is higher compared to pristine PBTTT.

6.3.Conclusions

In conclusion, a synergistic effect between a high-mobility p-type OSP with a rigid backbone, PBTTT and DPPCN, a NIR dye molecule, has been systematically investigated, aiming towards developing high-performing OFETs and OPTs. It has been found that

blending/doping an optimum percentage (2%) of DPPCN in the PBTTT matrix improved the overall crystalline order of the film, along with an enhanced uniaxial molecular orientation. The exciton bandwidth was also found to be the lowest (29.4 meV) in the optimum hybrid material. Results from XRD and HR-TEM justified the crystallinity improvement in the hybrid system. The KPFM results show an interesting uniaxial alignment of ordered domains in the hybrid system that facilitates enhanced average saturation mobility up to 0.2 cm^2/Vs in PBTTT/DPPCN(2%) compared to 0.16 cm^2/Vs in the pristine one. Moreover, the presence of an optimum percentage of a NIR-sensitive molecule in the system causes the inception of NIR sensitivity in the order of 10^3 and almost one order enhancement in photosensitivity for the red light, ~10^4. Thus, the present systematic investigation provides an insight into the synergistic effect (charge-transfer) in an OSP/NIR dye system with a high photo-sensing capability, which should inspire the chemists to design and develop highly efficient conjugated systems suitable for high-performing OPTs.